Local structural distortions in strained $Ba_{0.5}Sr_{0.5}TiO_3$ thin films

J. C. Woicik and E. L. Shirley
National Institute of Standards and Technology, Gaithersburg, Maryland 20899, USA

K. Gilmore
European Synchrotron Radiation Facility (ESRF), Boîte Postale 220, F-38043 Grenoble, France

K. E. Andersen
National Research Council/U.S. Naval Research Laboratory, Washington, DC 20375, USA

C. Stephen Hellberg
U.S. Naval Research Laboratory, Washington, DC 20375, USA

(Received 23 May 2017; revised manuscript received 8 August 2017; published 28 September 2017)

The local atomic geometries in $Ba_{0.5}Sr_{0.5}TiO_3$ thin films grown on MgO(001) substrates have been determined by Ti 1*s* near-edge x-ray-absorption fine-structure measurements and density-functional-theory calculations. The accuracy of the atomic geometries predicted by density-functional theory is demonstrated by simulations of the near-edge x-ray-absorption fine-structure spectra using a Bethe-Salpeter treatment of the Ti 1*s* core-hole interaction in the films. Our results show that films with either $c > a$ or $c < a$ tetragonal lattice distortions have their polarization vectors rotated toward or away from the [001] film-normal or *c*-axis direction, respectively. Both distortions result locally in the monoclinic *r* phase of the strain-phase diagram of Pertsev *et al.* [Phys. Rev. Lett. **80**, 1988 (1998)], and the polarizations are rotated significantly larger than the geometry would suggest.

DOI: 10.1103/PhysRevB.96.104111

In 1998, Pertsev *et al.* introduced the "temperature-misfit-strain" phase diagram to describe the changes in temperature and order of ferroelectric phase transitions in epitaxial ferroelectric films grown on substrates with dissimilar lattice constants [1]. The diagrams are based on a phenomenological Landau-Devonshire model that includes the coupling of polarization and strain due to the clamping effect of the film by the substrate. Diagrams for several materials have been published including $BaTiO_3$ [1], $PbTiO_3$ [1], $SrTiO_3$ [2], and $PbZr_{0.5}Ti_{0.5}O_3$ [3]. The diagrams predict the increase of Curie temperature observed in ferroelectric thin films [4–8], in addition to the different phases and polarization states that arise due to the lower symmetries often associated with epitaxial growth [9]. For example, the prototypical ferroelectric $BaTiO_3$ in its rhombohedral phase becomes monoclinic when strained to the in-plane lattice constant of a cubic substrate [1].

The work of Pertsev *et al.* spurred a flurry of first-principles calculations of misfit-strain-phase diagrams using density-functional theory (DFT) [10–13]. These calculations revealed the sensitivity of the phenomenological theory to the fitting of the model parameters used, and they also corrected the predictions of nonexistent phases [10]. First-principles modeling has the advantage of determining local atomic geometries within the films that ultimately drive their macroscopic behavior [14,15]. First-principles modeling is also applicable to engineered systems such as alloys, superlattices, and nanostructures for which model parameters do not exist [9,16–18].

Despite the one-to-one correspondence between microscopic structure and macroscopic behavior, there has been relatively little experimental work aimed at determining the exact atomic coordinates associated with a particular strain-phase relation in ferroelectric thin films. In practice, strain-dependent phenomena can be inferred from macroscopic properties, such as thin-film lattice constants or electrical measurements of polarization, but they do not directly determine local atomic geometries. In fact, scanning-probe microscopy [16], which is one of the often utilized nanometer-scale probes for the study of ferroelectric phase transitions, determines only the polarization state of film surfaces. In addition, local-structure measurements using x-ray or neutron diffraction [19] typically require bulk ceramics or single crystals and not thin films on account of their complex texture.

In this work, we demonstrate that near-edge x-ray-absorption fine-structure (NEXAFS) measurements can confirm the internal coordinates of a ferroelectric phase transition in ferroelectric thin films predicted by first-principles theory. As errors in the DFT computation of lattice constants are typically in the $\pm 1\%$ range (and hence comparable to ferroelectric strain effects), an approximation commonly used in such calculations is to set either the translation vectors or the volume of the unit cell to their experimental, room-temperature values [9]. Such implementation of experimental quantities into first-principles modeling is often performed [20], and the comparison of the measured and calculated spectra puts our calculation of internal coordinates with lattice constants fixed at the experimental values to test.

Samples were selected from a group of well-characterized $Ba_{0.5}Sr_{0.5}TiO_3$ (BST) thin films ($\sim 0.5\,\mu$m) grown on MgO(001) substrates under different Ar and O partial pressures. The control of partial pressures allows the introduction of oxygen vacancies into the films to structurally and chemically engineer their bulk lattice constants and strain states. X-ray-diffraction measurements of the in- (a) and out- (c) of-plane lattice constants as well as electrical measurements on the samples have been reported previously [21]. Films with both $c > a$ and $c < a$ tetragonal lattice distortions were

 ©2017 American Physical Society

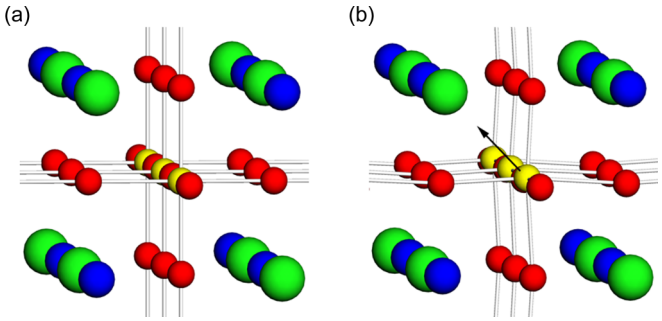

FIG. 1. (a) Structure of cubic, nonpolar BST. (b) Structure of cubic, polar BST calculated by DFT. Ba atoms are green, Sr atoms are blue, Ti atoms are yellow, and O atoms are red. The structure in (b) reveals the ferroelectric distortion with displacement of the Ti atoms along the [111] direction. Both structures are viewed slightly off of the [010] direction, and the Ti-displacement vector is shown in (b).

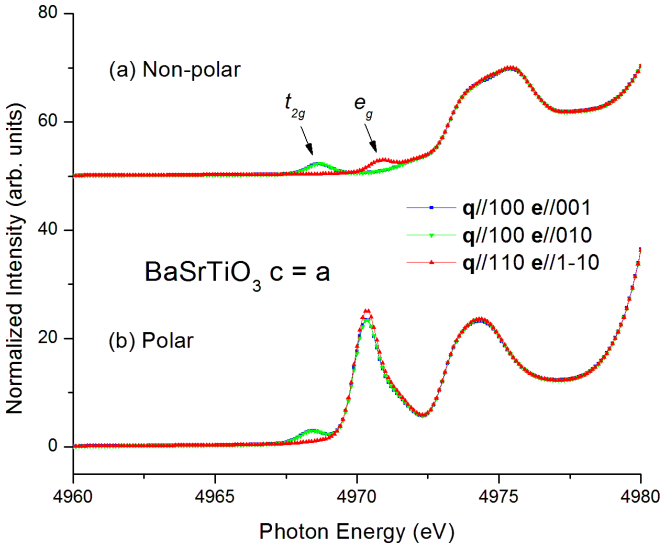

FIG. 2. Theoretical Ti $1s$ NEXAFS spectra for the two BST structures shown in Fig. 1. (a) Cubic, nonpolar BST. (b) Cubic, polar BST calculated by DFT. The t_{2g} and e_g transitions are indicated for the nonpolar structure.

chosen to elucidate the effects of both in-plane compressive and in-plane tensile strains on the local atomic geometries.

Figure 1(a) shows the ideal, *nonpolar* cubic perovskite structure of BST. Here Ba and Sr atoms occupy the corners of the cubic unit cells, Ti atoms are at the centers, and O atoms reside at the face centers in octahedral arrangement around the Ti atoms. To understand the local atomic distortions of this structure, we performed DFT calculations using the generalized-gradient approximation [22] and projected-augmented wave functions as implemented in the Vienna *ab initio* simulation package (VASP) [23]. Calculations were performed using the average bulk cubic lattice constant of the films equal to 4.024 Å. The in- and out-of-plane lattice constants were constrained at this value, while the internal coordinates of the BST were relaxed according to the Hellman-Feynman theorem. We find the lowest energy structure for BST with cubic translation vectors is polar, having the Ti atoms displaced along the [111] direction as shown in Fig. 1(b), with the arrow drawn to indicate the direction of Ti off-center displacement [24].

In anticipation of measuring the strain-dependent electronic structures of the films, we calculated the Ti $1s$ NEXAFS spectra for bulk crystals of BST with the measured cubic lattice constant and the local atomic geometries shown in Fig. 1; i.e., the ideal, nonpolar cubic structure and the relaxed polar cubic structure determined by DFT. The x-ray near-edge extinction coefficient $\mu(\varepsilon) = -\mathrm{Im}\langle 0|O[\varepsilon + i\gamma(\varepsilon) - H]^{-1}O|0\rangle$ involves the ground state $|0\rangle$, light-matter interaction O, and core-excited Hamiltonian H. H includes electron dynamics (through the band structure), the core-level binding energy, and electron core-hole excitonic effects [25,26]. We calculated $\mu(\varepsilon)$ using a Bethe-Salpeter treatment [27]. The broadening $\gamma(\varepsilon)$ simulated experimental resolution, electron-damping effects [28], state-dependent Franck-Condon effects [29], and other observed broadening. We used norm-conserving pseudopotentials with Ti $3s/3p$, Sr $4s/4p$, and Ba $5s/5p$ treated as valence electrons and an 81 Ry plane-wave cutoff. We sampled the full Brillouin zone at 216 k points, which was well converged, and about 60 conduction bands for 10-atom unit cells, which was ample for the spectral region presented. It should be noted that with the relative core binding energy not being exactly known theoretically, the absolute energy scale of the theoretical spectrum always requires a shift, which we realized simply by aligning the energies of the prominent e_g peak when comparing theory and experiment.

Theoretical spectra for cubic BST are presented in Fig. 2. They are plotted for different unit-cell orientations relative to the synchrotron-beam wave vector $\boldsymbol{q}$ and synchrotron-beam polarization vector $\boldsymbol{\varepsilon}$. The first two peaks in the spectra from cubic, nonpolar BST are dipole-forbidden (quadrupolar) transitions of the Ti $1s$ electrons to the Ti $3d$ derived t_{2g} (d_{xy}, d_{yz}, and d_{zx}) and e_g ($d_{3z^2-r^2}$ and $d_{x^2-r^2}$) unoccupied molecular orbitals [30]. The quadrupolar selection rules are evident from the figure [31]. The energy difference between the two peaks is 2.2 eV, which represents the crystal-field splitting [32]. The splitting results from the different orbital overlap between the Ti $3d$ orbitals and the ligand $2p$ orbitals that are strong functions of symmetry. These transitions appear sharp, rather than bandlike, due to excitonic interaction between the Ti $1s$ core hole and electron in the Ti $3d$ levels.

The intensity of the $1s$ to e_g transition has been shown to be enhanced by an amount proportional to the square of the component of the Ti displacement that resides along the synchrotron-beam x-ray polarization direction [33,34]. This enhancement is due to the dipole character introduced by chemical hybridization of the Ti $4p$ and $3d$ states in systems with broken inversion symmetry [32], and such a comparison of near-edge spectra is particularly sensitive to the TiO_6 cage structure and its distortions because of the effects on peak intensities. Consequently, the intensity of this transition has been used to assess the ferroelectric distortion in several perovskite systems [35]. Note the large enhancement of the $1s$ to e_g transition for the theoretical polar structure with polarization (i.e., Ti off-center displacement) along the [111] direction. Because the displacement of the Ti atoms is along the [111] direction, the intensity of the e_g peak for the

TABLE I. Room-temperature lattice parameters for cubic and tetragonally distorted BST (see text). Also shown are the results of the DFT calculations for the Ti displacement (in spherical coordinates) from the center of the unit cell that is defined by the oxygen coordinates. For $c = a$, the structure is cubic, while for $c \neq a$, the structure is monoclinic.

Distortion	a (Å)	c (Å)	r (Å)	θ (deg)	ϕ (deg)
$c = a$	4.024	4.024	0.197	54.74	45.00
$c > a$	4.002	4.039	0.186	45.70	45.00
$c < a$	4.037	4.014	0.203	59.88	45.00

polar structure shows relatively little angular dependence—the intrinsic quadrupolar selection rules add only a small contribution to the large, off-center electronic enhancement. This displacement also results in a relatively large shift of the e_g peak to lower photon energy, because the Ti e_g orbitals no longer point directly at the negatively charged oxygen ligands.

In order to determine the structure of the actual films measured, calculations were performed for films with the experimentally determined in- and out-of-plane lattice constants given in Table I and direct lattice vectors $\mathbf{R_1} = (a,0,c)$, $\mathbf{R_2} = (-a,0,c)$, and $\mathbf{R_3} = (0,-a,-c)$. These lattice constants correspond to in- and out-of-plane strains equal to $\varepsilon_a = -0.48\%$ and $\varepsilon_c = 0.44\%$ for the film with $c > a$, and $\varepsilon_a = 0.30\%$ and $\varepsilon_c = -0.27\%$ for the film with $c < a$, respectively. The calculations find the lowest-energy structures have the BST growing in its monoclinic phase, with the resulting Ti displacements (in spherical coordinates: r,θ,ϕ) from the center of the unit cell as given in Table I. When plotted as in Fig. 1(b), structural differences between the cubic and strained films appear negligible on this scale. Consequently, all structural distortions will be described in terms of the Ti-displacement vector.

Figures 3 and 4 show the Ti 1s NEXAFS spectra for the BST thin films. The data were recorded at the National Institute of Standards and Technology beamline X23A2 at the National Synchrotron Light Source. For both the theoretical and experimental spectra, the data are plotted for different sample orientations relative to the synchrotron-beam wave vector $\boldsymbol{q}$ and synchrotron-beam polarization vector $\boldsymbol{\varepsilon}$. Glancing spectra were recorded within a few degrees of true glancing incidence. The data have been normalized to equal edge jump. All data were acquired at room temperature by measuring the Ti K_α fluorescence emission with a single-element SiLi detector aligned along the direction of synchrotron-beam polarization. The photon energy of the Si(311) double-crystal monochromator was scanned across the Ti 1s edge, and the fluorescence emission was normalized to the incident flux as determined by a nitrogen-filled ionization chamber upstream of the sample.

Note the large enhancement of the 1s to e_g transition at approximately $h\nu = 4970.4$ eV for both films compared to the theoretical spectra for cubic, nonpolar BST. There is also significant geometry dependence for both films compared to the theoretical spectra for cubic, polar BST: The transition is amplified for the film with $c > a$ when the synchrotron polarization is aligned out of plane and suppressed when the polarization is aligned in plane. The converse is true for the film with $c < a$.

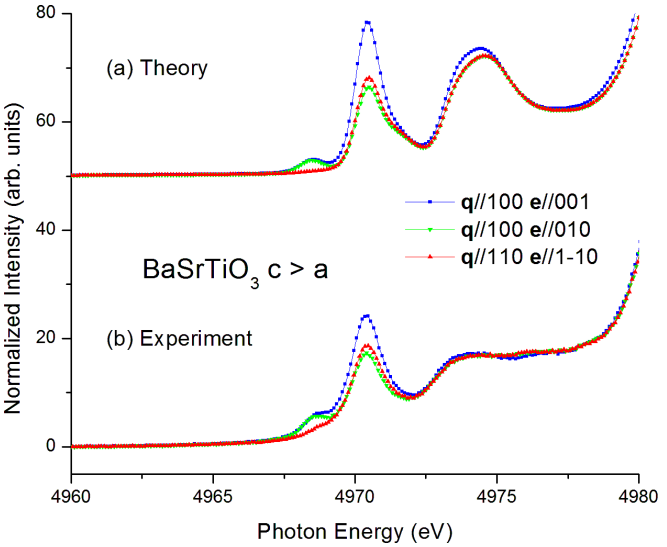

FIG. 3. Ti 1s NEXAFS spectra for BST with $c > a$. (a) Theory. (b) Experiment. Data have been normalized to unit step height and offset for clarity. The Ti-displacement vector [shown in Fig. 1(b)] is rotated toward the [001] direction. The measured and calculated e_g peaks have been energetically aligned.

To determine whether or not the DFT calculations accurately describe the local structures within the films, Figs. 3 and 4 also show the theoretical Ti 1s NEXAFS spectra calculated using the local atomic coordinates determined by DFT for the strained films. Remarkably, all features of the electronic structure and its differences are reproduced in the theoretical calculations: relative energy shifts of the Ti 3d levels, t_{2g} and e_g in-plane angle dependence, and orientation enhancement of

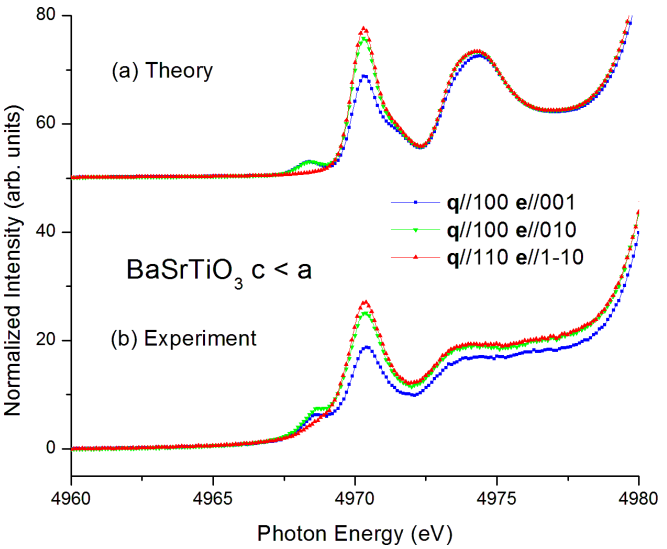

FIG. 4. Ti 1s NEXAFS spectra for BST with $c < a$. (a) Theory. (b) Experiment. Data have been normalized to unit step height and offset for clarity. The Ti-displacement vector [shown in Fig. 1(b)] is rotated away from the [001] direction. The measured and calculated e_g peaks have been energetically aligned.

the $1s$ to e_g transition. In fact, the only discrepancy between the first-principles theory and experiment is the relative intensity of the feature occurring above 4973 eV, which may, in part, be due to our neglect of chemical disorder on the Ba and Sr sites. We note, however, that this discrepancy is common even in calculations of bulk (nonalloyed) $SrTiO_3$ and $BaTiO_3$ [36]. Transitions to the t_{2g} and e_g orbitals are most sensitive to the local oxygen environment around the absorbing Ti atom [29]; i.e., the crystal field, and alloy disorder has been shown to have a negligible effect on them in other perovskite systems [37]. Nevertheless, it is satisfying to find that the calculations reproduce these features without the added complexity of alloy disorder.

We also performed DFT calculations for planar and columnar BST structures that are also supported by a 10-atom unit cell, and changes in the magnitude and orientation of the polarization were found to be negligible from the structure shown in Fig. 1. NEXAFS calculations for $BaTiO_3$ and $SrTiO_3$ with the same atomic positions as the alloy also found the spectra to be essentially identical.

From the raw NEXAFS data, it is clear that the films have their Ti displacements rotated away from the [111] direction. In the case of the film with $c > a$, the Ti displacement is rotated toward the [001] direction, and, conversely, in the case of the film with $c < a$, the Ti displacement is rotated away from the [001] direction. The fact that the intensity of the peak remains large for all directions indicates that the rotations are not completely in- or out-of-plane; i.e., the films are locally in the monoclinic r phase of Pertsev *et al.* [1] with film polarization equal to $P(\boldsymbol{i} + \boldsymbol{j}) + P_z\boldsymbol{k}$ for both in-plane compressive and in-plane tensile strains. These conclusions have now been confirmed by first-principles calculation and our physical demonstration of its accuracy.

It is interesting to compare the distortions predicted from simple geometric considerations and the DFT results. If we write $\hat{\boldsymbol{d}} = [a(\boldsymbol{i} + \boldsymbol{j}) + c\boldsymbol{k}]/(2a^2 + c^2)^{1/2}$ as the unit vector along a cell diagonal, computing $\cos^{-1}[\hat{\boldsymbol{d}}(a = c) \cdot \hat{\boldsymbol{d}}(a \neq c)]$ gives the angle of rotation of the displacement vector to first order in the strains [38,39]:

$$\Delta\theta = \frac{\sqrt{2}}{3}[\varepsilon_a - \varepsilon_c]. \tag{1}$$

Using the experimentally determined in- and out-of-plane lattice constants, Eq. (1) predicts a rotation of the polarization vector by 0.25° toward the c axis for the $c > a$ distortion and a rotation of the polarization vector by 0.15° away from the c axis for the $c < a$ distortion. We note that the rotation of the polarization vector as calculated by DFT is *over an order of magnitude* larger than predicted by Eq. (1). As the results of DFT agree so closely with the experimental NEXAFS spectra, it is clear that additional energetic effects associated with each phase transition must be responsible for the significantly larger distortions observed. These results are in accord with *ab initio* effective Hamiltonian results for $BaTiO_3$ that describe the rotation of the polarization vector with strain [10]. It was found that the rotation is second order in the strain; i.e., it is continuous until the strain reaches a critical value upon which the polarization resides completely in either the (001) or (110) planes.

Our findings reveal the broad region of existence of the monoclinic r phase at room temperature predicted by first principles for both compressive and tensile strains [10]. They also indicate the small energy cost of polarization rotation that has been used to explain the enhancement of both piezoelectric and dielectric responses [11,14,40,41]. This work also supports the conclusions of Stern [34] who, by considering the relative time scales of their excitations, resolved the apparent discrepancy between XAFS [35] and nuclear magnetic-resonance measurements [42] concerning the order/disorder nature of the tetragonal ferroelectric to cubic paraelectric phase transition in $BaTiO_3$. The unit cell of $BaTiO_3$ (and BST) in its cubic, high-temperature phase has the Ti atoms displaced along the eight equivalent [111] directions, and small (<1%), tetragonal distortions of the unit cell lead to relatively large ($\gtrsim$4°) rotations of the Ti-displacement vector either toward or away from the c axis. Interestingly, the magnitudes of the displacements do not appear to be affected significantly by these levels of in-plane strain.

In conclusion, we have examined the local atomic distortions in strained BST films grown on MgO substrates with either in-plane tensile or in-plane compressive strains. We find agreement between Ti $1s$ NEXAFS spectra and electronic structure calculations utilizing the local atomic distortions determined by DFT for both the direction and magnitude of the spontaneous polarization. The films are locally in the r phase of Pertsev *et al.* [1], supporting the broad range of r phase stability predicted by model Hamiltonian calculations [10].

This work was performed at the National Synchrotron Light Source (Brookhaven National Laboratory) beamline X23A2 of the National Institute of Standards and Technology. Use of the National Synchrotron Light Source was supported by the U.S. Department of Energy, Office of Basic Energy Sciences, under Contract No. DE-AC02-98CH10886. Additional support was provided by the National Institute of Standards and Technology and the Office of Naval Research through the Naval Research Laboratory's Basic Research Program. The work was supported in part by a grant of computer time from the DoD High Performance Computing Modernization Program.

[1] N. A. Pertsev, A. G. Zembilgotov, and A. K. Tagantsev, Phys. Rev. Lett. **80**, 1988 (1998).

[2] N. A. Pertsev, A. K. Tagantsev, and N. Setter, Phys. Rev. B **61**, R825 (2000).

[3] N. A. Pertsev, V. G. Kukhar, H. Kohlstedt, and R. Waser, Phys. Rev. B **67**, 054107 (2003).

[4] G. A. Rossetti, L. E. Cross, and K. Kushida, Appl. Phys. Lett. **59**, 2524 (1991).

[5] Y. Yoneda, T. Okabe, K. Sakaue, H. Terauchi, H. Kasatani, and K. Deguchi, J. Appl. Phys. **83**, 2458 (1998).
[6] S. K. Streiffer, J. A. Eastman, D. D. Fong, C. Thompson, A. Munkholm, M. V. Ramana Murty, O. Auciello, G. R. Bai, and G. B. Stephenson, Phys. Rev. Lett. **89**, 067601 (2002).
[7] K. J. Choi, M. Biegalski, Y. L. Li, A. Sharan, J. Schubert, R. Uecker, P. Reiche, Y. B. Chan, X. Q. Pan, V. Gopalan, L.-Q. Chen, D. G. Schlom, and C. B. Eom, Science **306**, 1005 (2004).
[8] J. H. Haeni, P. Irvin, W. Chang, R. Uecker, P. Reiche, Y. L. Li, S. Choudhury, W. Tian, M. E. Hawley, B. Craigo, A. K. Tagantsev, X. Q. Pan, S. K. Streiffer, L. Q. Chen, S. W. Kirchoefer, J. Levy, and D. G. Schlom, Nature (London) **430**, 758 (2004).
[9] M. Dawber, K. M. Rabe, and J. F. Scott, Rev. Mod. Phys. **77**, 1083 (2005).
[10] O. Diéguez, S. Tinte, A. Antons, C. Bungaro, J. B. Neaton, K. M. Rabe, and D. Vanderbilt, Phys. Rev. B **69**, 212101 (2004).
[11] C. Bungaro and K. M. Rabe, Phys. Rev. B **69**, 184101 (2004).
[12] O. Diéguez, K. M. Rabe, and D. Vanderbilt, Phys. Rev. B **72**, 144101 (2005).
[13] A. Antons, J. B. Neaton, K. M. Rabe, and D. Vanderbilt, Phys. Rev. B **71**, 024102 (2005).
[14] Z. Wu and H. Krakauer, Phys. Rev. B **68**, 014112 (2003).
[15] C. S. Hellberg, K. E. Andersen, H. Li, P. J. Ryan, and J. C. Woicik, Phys. Rev. Lett. **108**, 166101 (2012).
[16] C. H. Ahn, K. M. Rabe, and J.-M. Triscone, Science **303**, 488 (2004).
[17] J. F. Scott, Science **315**, 954 (2007).
[18] D. G. Schlom, L.-Q. Chen, C.-B. Eom, K. M. Rabe, S. K. Streiffer, and J.-M. Triscone, Annu. Rev. Mater. Res. **37**, 589 (2007).
[19] G. H. Kwei, A. C. Laswon, S. L. Billinge, and S.-W. Cheong, J. Phys. Chem. **97**, 2368 (1993).
[20] Z. Wu, G. Sághi-Szabó, R. E. Cohen, and H. Krakauer, Phys. Rev. Lett. **94**, 069901(E) (2005).
[21] L. M. Alldredge, J. C. Woicik, W. Chang, S. W. Kirchoefer, and J. M. Pond, Appl. Phys. Lett. **91**, 052909 (2007).
[22] J. P. Perdew, K. Burke, and M. Ernzerhof, Phys. Rev. Lett. **77**, 3865 (1996).
[23] G. Kresse and J. Furthmüller, Phys. Rev. B **54**, 11169 (1996); G. Kresse and D. Joubert, *ibid.* **59**, 1758 (1999); P. E. Blöchl, *ibid.* **50**, 17953 (1994).
[24] I. Levin, V. Krayzman, and J. C. Woicik, Phys. Rev. B **89**, 024106 (2014).
[25] E. L. Shirley, Ultramicroscopy **106**, 986 (2006).
[26] E. L. Shirley, J. Electron Spectrosc. Relat. Phenom. **144–147**, 1187 (2005).
[27] E. L. Shirley, J. Electron Spectrosc. Relat. Phenom. **136**, 77 (2004).
[28] E. L. Shirley, J. A. Soininen, and J. J. Rehr, in *Optical Constants of Materials for UV to X-ray Wavelengths*, edited by Regina Soufli and John F. Seely, Proceedings of SPIE Vol. 5538 (SPIE, Bellingham, WA, 2004), p. 125.
[29] F. M. F. de Groot, J. C. Fuggle, B. T. Thole, and G. A. Sawatzky, Phys. Rev. B **41**, 928 (1990).
[30] J. C. Woicik, E. L. Shirley, C. S. Hellberg, K. E. Andersen, S. Sambasivan, D. A. Fischer, B. D. Chapman, E. A. Stern, P. Ryan, D. L. Ederer, and H. Li, Phys. Rev. B **75**, 140103(R) (2007).
[31] C. Brouder, J. Phys.: Condens. Matter **2**, 701 (1990).
[32] F. A. Cotton, *Chemical Applications of Group Theory*, 2nd ed. (Wiley-Interscience, New York, 1971), Chap. 9.
[33] R. V. Vedrinskii, V. L. Kraizman, A. A. Novakovich, Ph. V. Demekhin, and S. V. Urazhdin, J. Phys.: Condens. Matter **10**, 9561 (1998).
[34] E. A. Stern, Phys. Rev. Lett. **93**, 037601 (2004).
[35] B. Ravel, E. A. Stern, R. I. Vedrinskii, and V. Kraizman, Ferroelectrics **206**, 407 (1998).
[36] T. Yamamoto, T. Mizoguchi, and I. Tanaka, Phys. Rev. B **71**, 245113 (2005).
[37] V. Krayzman, I. Levin, J. C. Woicik, D. Yoder, and D. A. Fischer, Phys. Rev. B **74**, 224104 (2006).
[38] J. C. Woicik, C. E. Bouldin, K. E. Miyano, and C. A. King, Phys. Rev. B **55**, 15386 (1997).
[39] J. C. Woicik, Surf. Sci. Rep. **69**, 38 (2014).
[40] S. E. Park and T. R. Shrout, J. Appl. Phys. **82**, 1804 (1997).
[41] H. X. Fu and R. E. Cohen, Nature (London) **403**, 281 (2000).
[42] B. Zalar, V. V. Laguta, and R. Blinc, Phys. Rev. Lett. **90**, 037601 (2003).